Title

Ferrocene-bis(phosphinimine) Nickel(II) and Palladium(II) Alkyl Complexes: Influence of the Fe-M (M = Ni and Pd) Interaction on Redox Activity and Olefin Coordination

Journal

ORGANOMETALLICS, 36(22)

ISSN

0276-7333

Authors

Abubekerov, M
Khan, SI
Diaconescu, PL

Publication Date

2017-11-27

DOI

10.1021/acs.organomet.7b00626

Peer reviewed

Ferrocene-bis(phosphinimine) Nickel(II) and Palladium(II) Alkyl Complexes: Influence of the Fe-M (M = Ni, Pd) Interaction on Redox Activity and Olefin Coordination

Mark Abubekerov, Saeed I. Khan, and Paula L. Diaconescu*

Department of Chemistry and Biochemistry, University of California, Los Angeles, CA 90095

Supporting Information Placeholder

ABSTRACT: The synthesis of several novel nickel(II) and palladium(II) ferrocene-bis(phosphinimine) alkyl complexes containing iron-nickel and iron-palladium interactions is reported. The redox behavior of all complexes was evaluated electrochemically and chemically; in addition, reactions with weak nucleophiles, such as acetonitrile and olefins, were also investigated. DFT calculations were performed to understand the electronic structure of the alkyl metal complexes.

INTRODUCTION

Catalytic processes that can be switched by an external stimulus can offer an additional, 'bio-like' control of chemical transformations.[1-2] Early examples showed that switchable catalysts could be used to speed up or slow down the rate of a reaction according to the presence of a specific trigger,[3-12] which could be either a physical or a chemical stimulus,[1-2, 13] or to change the stereochemical[14-16] outcome of a reaction (on/off switches). In recent years, however, more advanced tasks have been accomplished, such as turning 'on' and 'off' different forms of the same pre-catalyst in order to promote complementary reactions that take place from a mixture of different building blocks.[17-23] Redox switchable catalysis uses redox reagents (chemical triggers) to turn on and off reactions. The earlier works of Wrighton et el.,[12] Long et al.,[3] and Plenio et al.[5] illustrated the influence of the redox states of ferrocenyl units, in supporting ligands, on catalysis. Our initial work focused extensively on utilizing ferrocene-based ligands for the redox control of ring-opening polymerizations (ROP) of cyclic esters. Starting with indium, yttrium,[4] and cerium[24] phosfen (phosfen = 1,1'-di(2-*tert*-butyl-6-diphenylphosphiniminophenoxy)ferrocene) complexes, an on/off activity for the polymerization of L-lactide was observed based on the oxidation state of the iron center. These early efforts culminated in the discovery of a system that displayed redox-controlled polymerization of several cyclic monomers: first in the case of L-lactide/ε-caprolactone with a titanium thiolfan complex, (thiolfan*)Ti(O^{i}Pr)$_2$ (thiolfan* = 1,1'-di(2,4-di-*tert*-butyl-6-thiophenoxy)ferrocene),[18] and then for L-lactide/cyclohexene oxide utilizing a zirconium salfan complex, (salfan)Zr(O^{t}Bu)$_2$ (salfan = 1,1'-di(2-*tert*-butyl-6-*N*-methylmethylenephenoxy)ferrocene).[17]

Recently, there have been efforts by our group and others to expand the application of redox-controlled systems beyond ROP.[10] Such examples include ferrocene-based ligands capable of modulating monomer selectivity in palladium systems for olefin polymerization[25-27] and Buchwald-Hartwig cross-coupling reactions,[28] utilization of cobalt complexes for olefin hydroalkoxylation,[29] and of gold mesoionic carbenes for heterocycles synthesis.[30] However, in all cases of redox-controlled catalysis, the ferrocene unit is distant from the primary metal center and no direct interaction exists between iron in ferrocene and the metal involved in a substrate transformation.

Various bidentate ferrocene derived ligands reported in the literature containing phosphorus,[31-37] sulfur,[38-41] and nitrogen-based[42-53] substituents are known to promote direct iron-metal interactions. However, the use of these complexes in redox-switchable catalysis has not been investigated. For example, ferrocene-bis(phosphinimines) have been used as supporting ligands,[43, 54] but not in catalytic examples. Based on our interest in redox-switchable catalysis utilizing ferrocene derivatives, we decided to prepare ferrocene-bis(phosphinimine) nickel and palladium alkyl complexes containing iron-nickel and iron-palladium interactions and investigate their efficacy for redox-switchable olefin polymerization.

RESULTS AND DISCUSSION

Preparation and characterization of the ferrocene-bis(phosphinimine) metal complexes. Initial attempts to carry out a direct ligand substitution using fc(NPPh$_3$)$_2$ to prepare the halide-alkyl complexes of nickel and palladium were unsuccessful (Scheme 1). However, the addition of NaBPh$_4$ to (PPh$_3$)$_2$NiCl(Ph) or (COD)PdCl(Me) (COD = 1,5-cyclooctadiene) in the presence of fc(NPPh$_3$)$_2$ in methylene chloride resulted in the isolation of [fc(NPPh$_3$)$_2$NiPh][BPh$_4$] and [fc(NPPh$_3$)$_2$PdMe][BPh$_4$] as red crystals in an 82.4% yield and orange crystalline material in 67.0% yield, respectively (Scheme 1). The solid-state molecular structures of [fc(NPPh$_3$)$_2$NiPh][BPh$_4$] (Figure 1) and [fc(NPPh$_3$)$_2$PdMe][BPh$_4$] (Figure 2) were investigated using single-crystal X-ray diffraction. The coordination environments around the nickel and palladium centers have a distorted square planar geometry with a τ value[55] of 0.18 and 0.16, respectively.

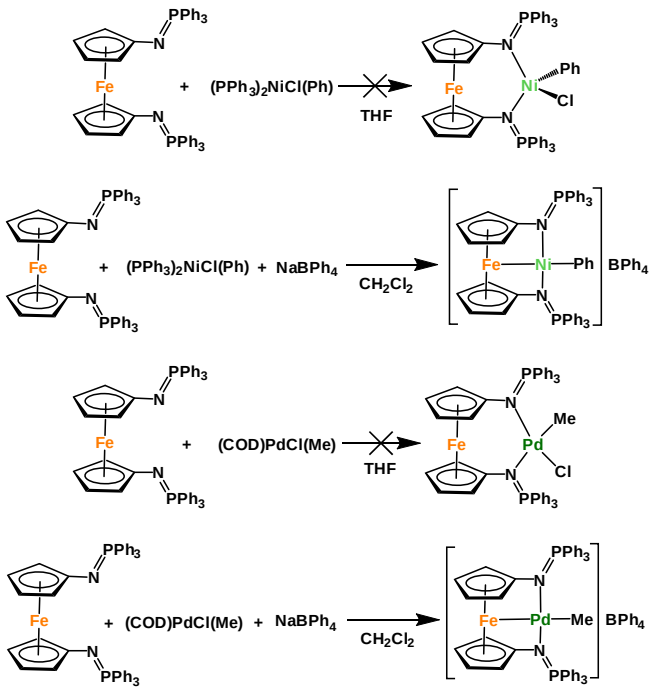

Scheme 1. The preparation of nickel and palladium ferrocene-bis(triphenylphosphinimine) complexes.

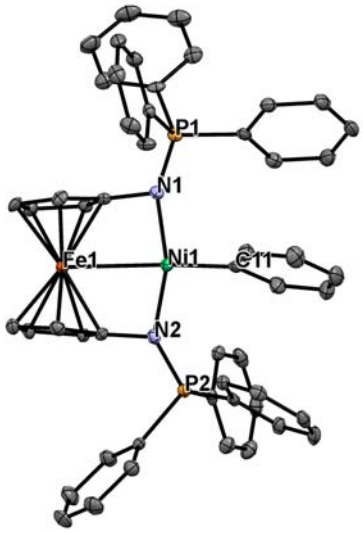

Figure 1. Molecular structure drawing of [fc(NPPh$_3$)$_2$NiPh][BPh$_4$] with thermal ellipsoids at 50% probability; hydrogen, solvent, and borate atoms are omitted for clarity. Selected distances (Å) and angles (°): N(1)-P(1), 1.613(2); N(2)-P(2), 1.613(2); N(1)-Ni(1), 1.898(2); N(2)-Ni(1), 1.895(2); C(11)-Ni(1), 1.891(3); Fe(1)-Ni(1), 2.8244(6); C(11)-Ni(1)-N(1), 102.4(1); C(11)-Ni(1)-N(2), 97.2(1); N(1)-Ni(1)-Fe(1), 80.94(6); N(2)-Ni(1)-Fe(1), 79.52(6).

The iron-nickel distance of 2.8244(6) Å is similar to that of a related complex [fc(S$_2$)Ni(PMe$_2$Ph)] (2.886(1) Å)[41] and longer than those observed for the dicationic species [fc(NIm)$_2$Ni(NCMe)][BF$_4$]$_2$ (2.6268(4) Å) and [fc(NIm)$_2$Ni(PMe$_3$)][BF$_4$]$_2$ (2.7376(4) Å, fc(NIm)$_2$ = *N,N'*-bis(1,3-di-*iso*-propyl-4,5-dimethylimidazolin-2-ylidene)-1,1'-ferrocenediamine).[44] The palladium-iron distance of 2.7957(5) Å is comparable with values reported for the similar complexes [fc(NIm)$_2$Pd(PMe$_3$)][BF$_4$]$_2$ (2.7475(4) Å), [fc(NIm)$_2$Pd(PMe$_3$)][BF$_4$]$_2$ (2.7424(3) Å),[44] [(dppf)Pd(PPh$_3$)][BF$_4$]$_2$ (2.877(2) Å, dppf = 1,1'-bis(diphenylphosphino)ferrocene),[56] [fc(S$_2$)Pd(PPh$_3$)] (2.878(1) Å)[39] and is longer than those observed for [fc(NIm)$_2$Pd(NCMe)][BF$_4$]$_2$ (2.6297(4) Å), [fc(NIm)$_2$Pd(PPh$_3$)][BF$_4$]$_2$ (2.6447(3) Å),[44] and [fc(NPPh$_3$)$_2$Pd(Cl)][Cl] (2.67 Å).[43] The ^{1}H NMR spectrum of [fc(NPPh$_3$)$_2$NiPh][BPh$_4$] is consistent with the presence in solution of a diamagnetic species and both the nickel and palladium complexes display a wide separation between the Cp signals (0.97 ppm and 1.46 ppm, respectively), consistent with the presence of an Fe-M (M = Ni, Pd) interaction.[43] In the ^{31}P NMR spectra, the chemical shifts of 37.5 ppm (nickel) and 30.2 ppm (palladium) are downfield compared to that of fc(NPPh$_3$)$_2$ (27.2 ppm).[43] The presence of the borate counter ion was confirmed by singlets at -5.7 ppm and -5.9 ppm for the nickel and palladium complexes, respectively, in the corresponding ^{11}B NMR spectra.

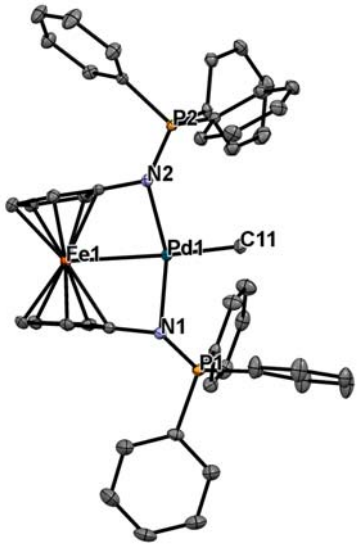

Figure 2. Molecular structure drawing of [fc(NPPh$_3$)$_2$PdMe][BPh$_4$] with thermal ellipsoids at 50% probability; hydrogen, solvent, and borate atoms are omitted for clarity. Selected distances (Å) and angles (°): N(1)-P(1), 1.620(1); N(2)-P(2), 1.606(1); N(1)-Pd(1), 2.072(1); N(2)-Pd(1), 2.031(1); C(11)-Pd(1), 2.051(2); Fe(1)-Pd(1), 2.7957(5); C(11)-Pd(1)-N(1), 102.29(6); C(11)-Pd(1)-N(2), 97.14(7); N(1)-Pd(1)-Fe(1), 81.07(4); N(2)-Pd(1)-Fe(1), 79.46(4).

Electrochemical studies performed on [fc(NPPh$_3$)$_2$NiPh][BPh$_4$] displayed a complicated and uninformative redox behavior (Figure S40). Attempts to perform a chemical oxidation using acetyl ferrocenium tetrakis(3,5-bis(trifluoromethyl)phenyl)borate ([^{Ac}Fc][BAr^F], Scheme 2 and Figure S26) or AgBF$_4$ (Figure S27) and a reduction using cobaltocene (Figure S24) on an NMR reaction scale did not result in the formation of any new species. Utilizing KC$_8$ as a reducing agent resulted only in the formation of nickel black and liberation of fc(NPPh$_3$)$_2$ (Scheme 2, Figure S25). On the other hand, electrochemical studies performed on [fc(NPPh$_3$)$_2$PdMe][BPh$_4$] (Figure S41) displayed several quasi-reversible redox processes in the range of 0 – 1.25 V (vs. Fc/Fc$^+$) suggesting that a more potent oxidant than a ferrocenium salt may be used. Similarly to the nickel case, utilizing [^{Ac}Fc][BAr^F] as an oxidant led to the

formation of several minor species, with the starting material remaining the predominant species (Scheme 2, Figure S28). However, in the presence of excess $AgBF_4$, the formation of a single species was observed in the ^{31}P NMR spectrum (Figure S37). A closer look at the in situ generated complex via ^{1}H, ^{11}B, and ^{19}F NMR spectroscopies (Figures S36 and S38-39) revealed the loss of the methyl group and the presence of tetrafluoroborate as the predominant counter ion in solution. The existence of palladium-fluorine interactions in the newly formed palladium complex, in the absence of a coordinating solvent, can be postulated based on the broad signals observed in the ^{19}F NMR spectrum. Scaling up the reaction and the addition of THF resulted in the isolation of $[fc(NPPh_3)_2Pd(THF)][BF_4]_2$ (Scheme 2) as dark golden plates in a 73.2% yield. The results of an X-ray diffraction study are displayed in Figure 3 along with selected distances and angles. The coordination environment around the palladium center is a distorted square planar geometry ($\tau = 0.14$). The palladium-iron distance of 2.6493(8) Å is significantly shorter than in $[fc(NPPh_3)_2PdMe][BPh_4]$ and is now comparable with those observed for $[fc(NIm)_2Pd(NCMe)][BF_4]_2$ (2.6297(4) Å), $[fc(NIm)_2Pd(PPh_3)][BF_4]_2$ (2.6447(3) Å),[44] and $[fc(NPPh_3)_2Pd(Cl)][Cl]$ (2.67 Å).[43] In the ^{1}H NMR spectrum, the separation between the Cp signals (1.76 ppm) is slightly larger (1.46 ppm) than for the parent complex, $[fc(NPPh_3)_2PdMe][BPh_4]$. In the ^{31}P NMR spectrum, the chemical shift of 37.4 ppm is downfield from that of $[fc(NPPh_3)_2PdMe][BPh_4]$ (30.2 ppm). The presence of the BF_4 ions was confirmed by ^{11}B NMR spectroscopy showing a singlet at -0.4 ppm and ^{19}F NMR spectroscopy showing two singlets at -152.0 and -152.1 ppm. The presence of two signals in the ^{19}F NMR spectrum is due to two naturally occurring boron isotopes, ^{11}B and ^{10}B, both of which are NMR active.

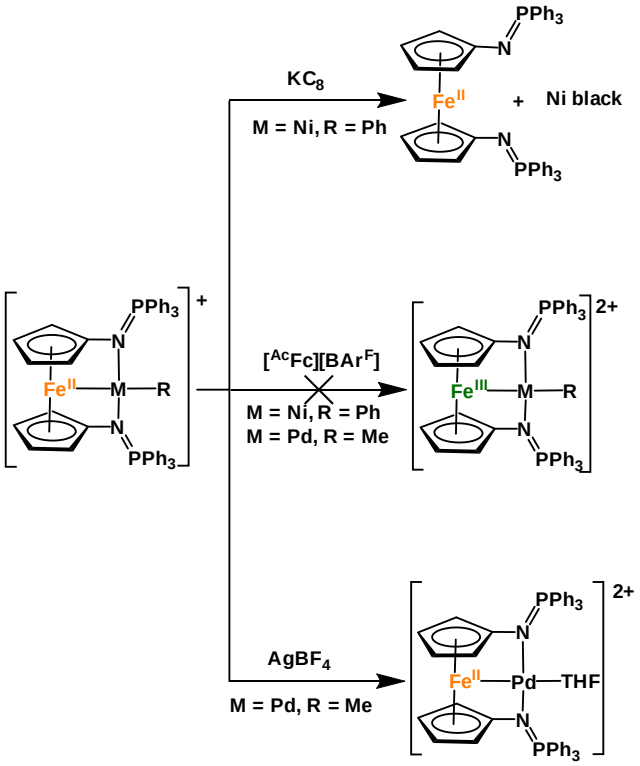

Scheme 2. Chemical oxidation and reduction of nickel and palladium ferrocene-bis(triphenylphosphinimine) complexes.

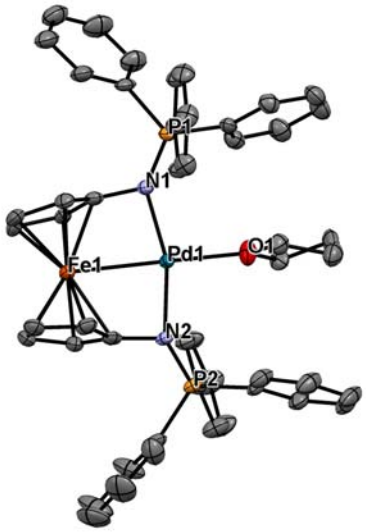

Figure 3. Molecular structure drawing of $[fc(NPPh_3)_2Pd(THF)][BF_4]_2$ with thermal ellipsoids at 50% probability; hydrogen, solvent, and borate atoms are omitted for clarity. Selected distances (Å) and angles (°): N(1)-P(1), 1.618(4); N(2)-P(2), 1.613(4); N(1)-Pd(1), 2.040(4); N(2)-Pd(1), 2.042(4); O(1)-Pd(1), 2.142(3); Fe(1)-Pd(1), 2.6493(8); O(1)-Pd(1)-N(1), 99.9(1); O(1)-Pd(1)-N(2), 97.7(1); N(1)-Pd(1)-Fe(1), 80.9(1); N(2)-Pd(1)-Fe(1), 81.5(1).

Next, we looked at the strength of the Fe-M (M = Ni, Pd) interaction. Previous reports by Cabrera et al.[31] and Jess et al.[44] showed that the Fe-M interactions in similar complexes are weak enough that a small molecule, such as acetonitrile, can disrupt them. The resulting acetonitrile adducts, in the case of palladium complexes, are non-symmetrical species that can be readily detected by heteronuclear NMR spectroscopy. Consequently, solutions of $[fc(NPPh_3)_2NiPh][BPh_4]$ and $[fc(NPPh_3)_2PdMe][BPh_4]$ in a mixture of acetonitrile and methylene chloride (1:1 vol %) both display singlets with no apparent shift, suggesting that the acetonitrile-palladium and acetonitrile-nickel interactions are not sufficient enough to overcome the metal-metal interactions in these complexes.

Due to the lack of redox activity in $[fc(NPPh_3)_2NiPh][BPh_4]$, we did not investigate its reactivity with olefins. On the other hand, although $[fc(NPPh_3)_2PdMe)[BPh_4]$ did not show a reversible redox process, we wanted to determine whether the comound would display the same redox behavior during a polymerization process. However, we did not observe any polymerization activity at ambient temperature in the reactions with ca. 100 equiv. of norbornene, styrene, 1-hexene, or ethylene (1.0 atm) in CD_2Cl_2, suggesting that the palladium-olefin interactions are also too weak to overcome the iron-palladium interaction. Elevating the reaction temperature resulted in the rapid formation of palladium black and no additional reactivity.

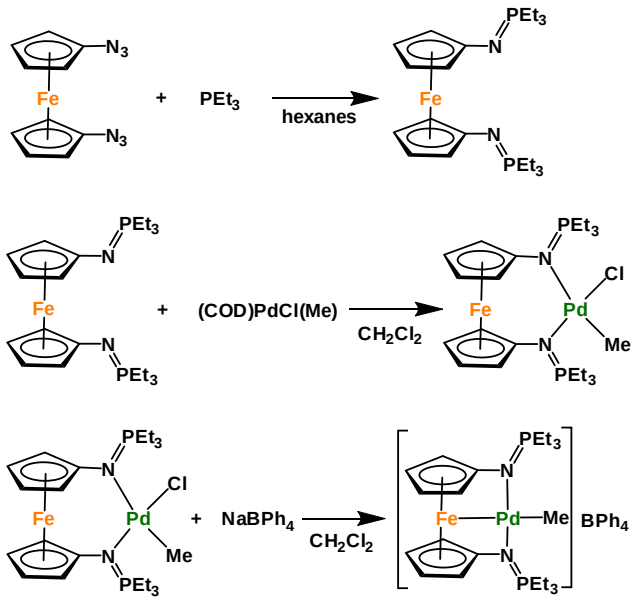

Scheme 3. The preparation of nickel and palladium ferrocene-bis(triethylphosphinimine) complexes.

The lack of activity of [fc(NPPh$_3$)$_2$PdMe][BPh$_4$] toward olefin polymerization prompted an investigation into alternative phosphinimine ligands. It is possible that a more electron rich derivative, such as the analogous tricyclohexylphosphinimine, would yield a palladium complex with a weaker Fe-Pd interaction.[43] However, we could not prepare [fc(NPCy$_3$)$_2$PdMe][BPh$_4$] (Scheme S1) although we used various methods, possibly due to the large steric bulk of the supporting ligand disfavoring the formation of a square planar fc(NPCy$_3$)$_2$PdCl(Me) intermediate. Alternatively, we prepared a new ferrocene-bis(phosphinimine) derivative, fc(PEt$_3$)$_2$ (Scheme 3), combining a more electron rich phosphine and a reduced steric environment compared with the fc(NPPh$_3$)$_2$ analogue. The reduction of the steric environment manifests itself in the isolation of a stable halide-alkyl complex, fc(NPEt$_3$)$_2$PdCl(Me) (Scheme 3) that was not achieved either with fc(NPPh$_3$)$_2$ or fc(NPCy$_3$)$_2$. The lack of symmetry in fc(NPCy$_3$)$_2$PdCl(Me) is clearly observed by a multitude of signals, specifically, the presence of eight separate signals (3.70 – 5.56 ppm) for the Cp protons in the ^{1}H NMR spectrum and two singlets (43.4 and 45.1 ppm) in the ^{31}P NMR spectrum.

Chloride abstraction from fc(NPEt$_3$)$_2$PdCl(Me) was accomplished with NaBPh$_4$ affording [fc(NPEt$_3$)$_2$PdMe][BPh$_4$] (Scheme 3) as an orange crystalline material in a 79.3% yield. The solid-state molecular structure of [fc(NPEt$_3$)$_2$PdMe][BPh$_4$] (Figure 4) was determined using single-crystal X-ray diffraction. The coordination environment around the palladium center is in a slightly distorted square planar geometry with a τ value of 0.20. The iron-palladium distance of 2.7806(5) Å is similar to that of [fc(NPPh$_3$)$_2$PdMe][BPh$_4$] (2.7957(5) Å). The ^{1}H NMR spectrum of [fc(NPEt$_3$)$_2$PdMe][BPh$_4$] shows a wide separation of 1.66 ppm between the signals of the Cp protons. A downfield shift in the resonance signal of [fc(NPEt$_3$)$_2$PdMe][BPh$_4$] (57.3 ppm) compared to both fc(NPEt$_3$)$_2$ (28.9 ppm) and fc(NPEt$_3$)$_2$PdCl(Me) (43.4 and 45.1 ppm) was observed in the ^{31}P NMR spectra. The BPh$_4$ ion appears at -5.7 ppm in the ^{11}B NMR spectrum, similar to the fc(NPPh$_3$)$_2$ nickel and palladium analogues.

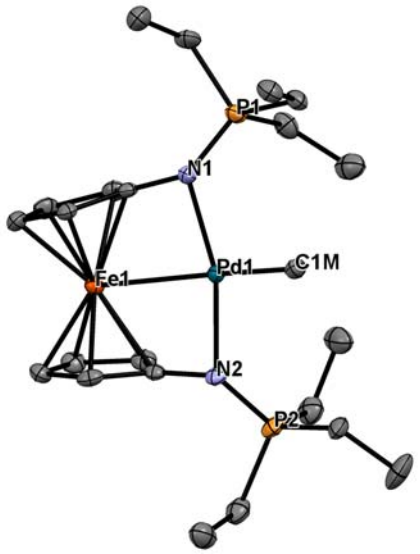

Figure 4. Molecular structure drawing of [fc(NPEt$_3$)$_2$PdMe][BPh$_4$] with thermal ellipsoids at 50% probability; hydrogen, solvent, and borate atoms are omitted for clarity. Selected distances (Å) and angles (°): N(1)-P(1), 1.624(2); N(2)-P(2), 1.612(2); N(1)-Pd(1), 2.054(2); N(2)-Pd(1), 2.046(2); C(1)M-Pd(1), 2.056(2); Fe(1)-Pd(1), 2.7806(5); C(1)M-Pd(1)-N(1), 99.4(1); C(1)M-Pd(1)-N(2), 98.35(9); N(1)-Pd(1)-Fe(1), 80.90(6); N(2)-Pd(1)-Fe(1), 81.02(6).

Electrochemical studies performed with [fc(NPEt$_3$)$_2$PdMe][BPh$_4$] displayed irreversible redox events similar to those for [fc(NPPh$_3$)$_2$PdMe][BPh$_4$] (Figure S43). Attempts to perform a chemical oxidation using excess AgBF$_4$ only resulted in a partial counter ion exchange while a new palladium species was not observed. The addition of acetonitrile to a methylene chloride solution of [fc(NPEt$_3$)$_2$PdMe][BPh$_4$] yielded the same results as were observed for [fc(NPPh$_3$)$_2$NiPh][BPh$_4$] and [fc(NPPh$_3$)$_2$PdMe][BPh$_4$]. No change in the chemical shift or formation of a non-symmetrical species was observed in the ^{31}P NMR spectrum. Furthermore, the species is thermally sensitive and gradually decomposes at ambient temperature to form a new major species (Figures S33-S34). A loss of the methyl group and the widening in the Cp proton separation was observed in the ^{1}H NMR spectrum as well as a further downfield shift of the signal in the ^{31}P NMR spectrum (Figures S34), reminiscent of the formation of [fc(NPPh$_3$)$_2$Pd(THF)][BF$_4$]$_2$ from [fc(NPPh$_3$)$_2$PdMe][BPh$_4$]. Decomposition was also clearly observed in the presence of styrene while no olefin-palladium interaction was observed at ambient temperature (Figure S35). Increasing the temperature only accelerated the rate of decomposition of the palladium-methyl species.

The lack of reactivity toward nucleophiles is not surprising when comparing the structural parameters of [fc(NPPh$_3$)$_2$PdMe][BPh$_4$] and [fc(NPEt$_3$)$_2$PdMe][BPh$_4$]. Although PEt$_3$ is a more electron rich phosphine than PPh$_3$, there are no significant observable differences in various distances or the geometries around palladium (Table 1). Therefore, in these two examples, a change in the phosphine substituent did not heavily impact the electronic properties of the resulting ferrocene-phosphinimine palladium complex. However, a decrease in the steric bulk of the phosphinimine ligand, upon a transition from a phenyl to an ethyl group, may explain the decrease in the

thermal stability of $[fc(NPEt_3)_2PdMe][BPh_4]$ and the observed loss of the methyl ligand.

Table 1. Summary of structural parameters and NMR spectroscopic data for nickel and palladium complexes.

	$[fc(NPPh_3)_2NiPh]^+$	$[fc(NPPh_3)_2PdMe]^+$	$[fc(NPPh_3)_2Pd(THF)]^{2+}$	$[fc(NPEt_3)_2PdMe]^+$
Fe-M (Å)	2.8244(6)	2.7957(5)	2.6493(8)	2.7806(5)
M-C (Å)	1.891(3)	2.051(2)	-	2.056(2)
M-N (Å)	1.895(2), 1.898(2)	2.031(1), 2.072(1)	2.040(4), 2.042(4)	2.046(2), 2.054(2)
N-P (Å)	1.613(2), 1.613(2)	1.606(1), 1.620(1)	1.613(4), 1.618(4)	1.612(2), 1.624(2)
τ	0.18	0.16	0.14	0.20
^{1}H NMR Cp-H (ppm)	3.39, 4.36	3.12, 4.58	3.63, 5.39	2.97, 4.63
^{11}B NMR (ppm)	-5.7	-5.9	-0.4	-5.7
^{31}P NMR (ppm)	37.5	30.2	37.4	57.3

DFT calculations. The extent of the Fe-M interaction can also be determined from DFT calculations. Geometry optimizations for $[fc(NPPh_3)_2NiPh]^+$, $[fc(NPPh_3)_2PdMe]^+$, and $[fc(NPEt_3)_2PdMe]^+$ were performed for the present study employing ADF2013.01, [57-59] using the PW91 functional[60] and no frozen electron cores. Although the counterion was omitted, all the atoms of the cations were included. The optimized Fe-M distances (Table 2) are close to each other and to the values obtained experimentally (Table S1). The calculated Mayer bond orders[61-62] are around 0.2 and are similar to the values obtained for other palladium complexes that show Fe-Pd interactions.[31-32, 35, 45]

Each of the analyzed compounds showed several molecular orbitals that indicate bonding interactions between iron and nickel or palladium (Figure 5 for selected orbitals and see the supporting information for more MOs for all three complexes, Figures S48, S50, and S52). Some of these orbitals are lying relatively deep, especially for the palladium complexes, for example, HOMO-16 and HOMO-25 for $[fc(NPPh_3)_2PdMe]^+$ and HOMO-13 for $[fc(NPEt_3)_2PdMe]^+$. Interestingly, the palladium complexes also contain π type iron-metal interactions, however, both the bonding and antibonding components are occupied (Figures S50 and S52).

In order to understand further the Fe→Pd interaction, natural bond orbital analysis was carried out using NBO 6.0[63] and the natural localized molecular orbitals (NLMOs) were generated (Figures S49, S51, and S53). All three metal complexes have two NLMOs with a bond order (BO) larger than 0.02: NLMO89 (BO = 0.04) and NLMO95 (BO = 0.03) for $[fc(NPPh_3)_2NiPh]^+$, NLMO93 (BO = 0.03) and NLMO219 (BO = 0.06) for $[fc(NPPh_3)_2PdMe)]^+$, and NLMO69 (BO = 0.03) and NLMO147 (BO = 0.06) for $[fc(NPEt_3)_2PdMe]^+$.

Topological analysis of the electron density was performed via Bader's atoms in molecule (AIM) theory.[64-65] AIM identifies bonds by calculating (3, −1) critical points, and it differentiates between covalent bonds and weak interactions, such as hydrogen bonds, van der Waals, and donor-acceptor interactions, by the value of the Laplacian ($\nabla^2\rho$). If $\nabla^2\rho < 0$, the interaction is considered covalent. If $\nabla^2\rho > 0$, the interaction is a weak interaction. AIM has been used to calculate bond critical points between two metal centers[66] and in ferrocene complexes.[67] All three $[fc(NPPh_3)_2NiPh]^+$, $[fc(NPPh_3)_2PdMe]^+$, and $[fc(NPEt_3)_2PdMe]^+$ species show Fe-M bond critical points (Table 1) consistent with a weak, non-covalent interaction (see the supporting information for details).

Table 2. Computational parameters for $[fc(NPPh_3)_2NiPh]^+$, $[fc(NPPh_3)_2PdMe]^+$, and $[fc(NPEt_3)_2PdMe]^+$.

	Ni	**Pd (PPh_3)**	**Pd (PEt_3)**
Fe-M (Å)	2.81	2.82	2.84
Fe-M Mayer Bond Order	0.21	0.27	0.27
Mulliken Charges			
Fe	-0.15	-0.13	-0.13
M	0.29	0.66	0.75
Hirshfeld Charges			
Fe	0.02	0.02	0.02
M	0.25	0.40	0.40
Wiberg bond index	0.09	0.10	0.10
NLMO Bond Order	0.09	0.09	0.09
Natural Charge			
Fe	0.14	0.17	0.17

M	0.70	0.58	0.58
Bader Charge			
Fe	0.66	0.71	0.71
M	0.59	0.39	0.39
ρ at Fe-M BCP[a]	0.03	0.03	0.03
Laplacian ($\nabla^2\rho$) at Fe-M BCP	0.04	0.05	0.05

[a] BCP is an Fe-M bond critical point (3, -1) identified by Bader analysis.

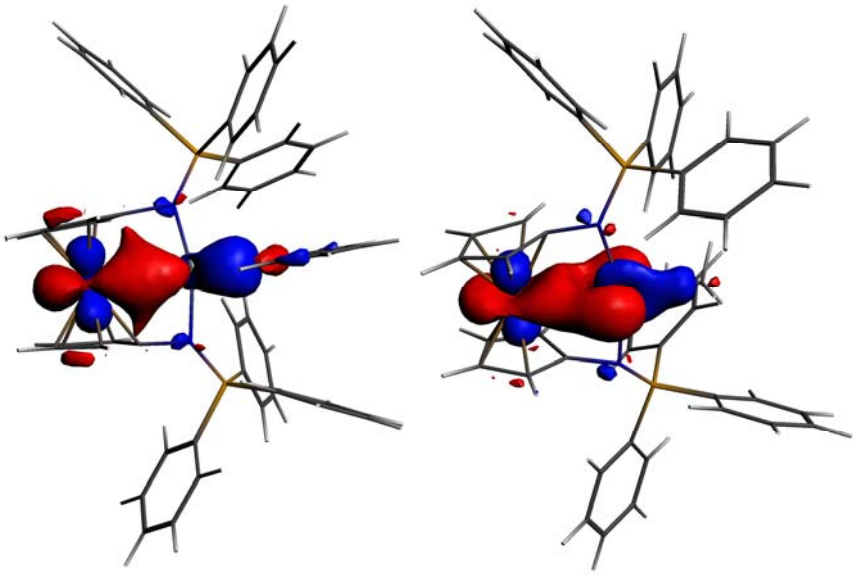

Figure 5. Frontier molecular orbitals: HOMO-6 for $[fc(NPPh_3)_2NiPh]^+$ (left) and HOMO-4 for $[fc(NPPh_3)_2PdMe]^+$ (right); isosurface value = 0.03.

Conclusions

The preparation of ferrocene-bis(phosphinimine) nickel and palladium alkyl complexes, via halide abstraction, was described. The ferrocene ligands are bound in a κ^3 fashion featuring iron-nickel and iron-palladium interactions. Electrochemically, only irreversible redox processes were observed for the palladium species. Chemically, $[fc(NPPh_3)_2NiPh][BPh_4]$ and $[fc(NPEt_3)_2PdMe][BPh_4]$ were redox inactive, while $[fc(NPPh_3)_2PdMe][BPh_4]$ underwent an irreversible oxidation resulting in the loss of the alkyl group. Attempts at disrupting the iron-palladium interactions using weak nucleophiles, such as acetonitrile and olefins, were unsuccessful. Although DFT calculations indicate that these interactions are relatively weak, they are important to the overall electronic stabilization of each metal complex, especially in the case of palladium. Based on the results of this study, the ferrocene-bis(phosphinimine) nickel and palladium alkyl complexes discussed herein are not viable for applications in redox-switchable olefin polymerization.

EXPERIMENTAL SECTION

General considerations. All reactions were performed using standard Schlenk techniques or in an MBraun drybox (<1 ppm O_2/H_2O) unless noted otherwise. All glassware, cannulas, and Celite were stored in an oven at > 425 K before being brought into the drybox. Solvents were purified using a two-column solid-state purification system by the method of Grubbs[68] and transferred to the glovebox without exposure to air. NMR solvents were obtained from Cambridge Isotope Laboratories, degassed, and stored over activated molecular sieves prior to use. NMR spectra were recorded at ambient temperature on Bruker AV-300, AV-500, and DRX-500 spectrometers unless otherwise noted. Proton and carbon chemical shifts are given relative to residual solvent peaks. Phosphorus, boron, and fluorine chemical shifts are given relative to external standards, H_3PO_4, $Et_2O{\cdot}BF_3$, and 1% Freon-113 in C_6D_6, respectively. Compounds $(PPh_3)_2NiClPh$,[69] (COD)PdCl(Me) (COD = 1,5-cyclooctadiene),[25] $fc(NPPh_3)_2$,[43] $fc(NPCy_3)_2$,[43] $fc(N_3)_2$,[70] $fc(NPCy_3)_2PdCl_2$,[43] and $[^{Ac}Fc][BAr^F]$[71] were prepared using literature procedures and, unless otherwise noted, all reagents were acquired from commercial sources and used as received. Elemental analysis of compounds $[fc(NPPh_3)_2NiPh][BPh_4]$, $[fc(NPPh_3)_2PdMe][BPh_4]$, $[fc(NPPh_3)_2Pd(THF)][BF_4]_2$, $fc(NPEt_3)_2$, and $[fc(NPEt_3)_2PdMe][BPh_4]$ was performed on an Exeter Analytical, Inc. CE-440 Elemental Analyzer. Elemental analysis of $[fc(NPPh_3)_2Pd(THF)][BF_4]_2$, $[fc(NPEt_3)_2PdMe][BPh_4]$, and $fc(NPEt_3)_2PdCl(Me)$ was carried out by Midwest Microlab, LLC, Indianapolis, IN.

$[fc(NPPh_3)_2NiPh][BPh_4]$. A solution of $fc(NPPh_3)_2$ (316.9 mg, 0.413 mmol) and $(PPh_3)_2NiClPh$ (261.5 mg, 0.375 mmol) in 10 mL of methylene chloride was added to a suspension of $NaBPh_4$ (128.6 mg, 0.375 mmol) in 5 mL of methylene chloride at 0 °C. The reaction mixture was stirred for 1 h at 0 °C followed by a filtration through a Celite plug. Volatile substances were removed under a reduced pressure and the remaining solids

were washed with diethyl ether (5 × 10 mL). The remaining solids were dissolved in 3 mL of methylene chloride, layered with 9 mL of diethyl ether, and stored for several hours at -35 °C. Decanting of the solution and washing with cold diethyl ether yielded the product as a red crystalline material. Recrystallization from methylene chloride/diethyl ether (1:3 vol %) layering at ambient temperature and washing with diethyl ether yielded analytically pure product (406.1 mg, 82.4%). X-ray quality crystals were obtained from methylene chloride/diethyl ether (1:3 vol %) layering at ambient temperature. Crystals of [fc(NPPh$_3$)$_2$NiPh][BPh$_4$] always contain a mixture of methylene chloride and diethyl ether per molecule of compound as supported by NMR data. ^{1}H NMR (CDCl$_3$, 500 MHz, 298 K): δ (ppm) 3.39 (t, 4H, Cp-*H*), 4.36 (t, 4H, Cp-*H*), 5.77 (t, 2H, Ni-(*m*-Ph)), 5.92 (t, 1H, Ni-(*p*-Ph)), 6.69 (d, 2H, Ni-(*o*-Ph)), 6.89 (t, 4H, B-(*p*-Ph)), 7.05 (t, 8H, B-(*m*-Ph)), 7.31-7.57 (m, 38H, B-(*o*-Ph), P-(*o*-Ph), P-(*m*-Ph), P-(*p*-Ph)). ^{13}C NMR (CDCl$_3$, 126 MHz, 298 K): δ (ppm) 69.0 (d, Cp-*C*), 72.4 (s, Cp-*C*), 80.6 (d, Cp-*C*), 121.6 (s, Ni*Ph*), 121.7 (s, B*Ph*), 124.8 (d, P*Ph*), 125.6 (m, B*Ph*), 125.7 (s, Ni*Ph*),128.9 (d, P*Ph*), 133.2 (d, P*Ph*), 133.5 (d, P*Ph*), 136.6 (s, B*Ph*), 138.9 (s, Ni*Ph*), 141.9 (s, Ni*Ph*), 164.5 (q, $^1J_{CB}$ = 49.9 Hz ,B-*C*). ^{11}B NMR (CDCl$_3$, 161 MHz, 298 K): δ (ppm) -5.7 (s). ^{31}P{^{1}H} NMR (CDCl$_3$, 203 MHz, 298 K): δ (ppm) 37.5 (s). Anal. Calcd: [fc(NPPh$_3$)$_2$NiPh][BPh$_4$]·(Et$_2$O)$_{0.5}$(CH$_2$Cl$_2$)(C$_{79}$H$_{70}$BCl$_2$FeN$_2$NiO$_{0.5}$P$_2$) C, 72.23; H, 5.37; N, 2.13. Found: C, 72.60; H, 5.33; N, 1.96.

[fc(NPPh$_3$)$_2$PdMe][BPh$_4$]. A solution of fc(NPPh$_3$)$_2$ (293.0 mg, 0.398 mmol) and (COD)PdCl(Me) (101.3 mg, 0.382 mmol) in 6 mL of methylene chloride was added to a suspension of NaBPh$_4$ (130.8 mg, 0.382 mmol) in 4 mL of methylene chloride at ambient temperature. The reaction mixture was stirred for 30 min at ambient temperature followed by a filtration through a Celite plug. Volatile substances were removed under a reduced pressure and the remaining solids were were dissolved in 3 mL of THF. Orange crystalline material forms from THF after several hours at ambient temperature. Decanting of the solution and washing with cold THF yielded the product as an orange crystalline material (319.6 mg, 67.0%). X-ray quality crystals were obtained from methylene chloride/diethyl ether vapor diffusion. Crystals of [fc(NPPh$_3$)$_2$PdMe][BPh$_4$] always contain a molecule of THF per molecule of compound as supported by NMR data. ^{1}H NMR (CD$_2$Cl$_2$, 500 MHz, 298 K): δ (ppm) -0.07 (s, 3H, Pd-C*H*$_3$), 3.12 (s, 4H, Cp-*H*), 4.58 (s, 4H, Cp-*H*), 6.86 (t, 4H, B-(*p*-Ph)), 7.01 (t, 8H, B-(*m*-Ph)), 7.31 (br s, 8H, B-(*o*-Ph)), 7.53 (m, 12H, P-(*o*-Ph)), 7.67 (t, 6H, P-(*p*-Ph)), 7.73 (m, 12H, P-(*m*-Ph)). ^{13}C NMR (CD$_2$Cl$_2$, 126 MHz, 298 K): δ (ppm) -4.7 (t, Pd-*C*H$_3$), 68.2 (d, Cp-*C*), 72.6 (s, Cp-*C*), 88.3 (d, Cp-*C*), 122.2 (s, B*Ph*), 126.1 (q, B*Ph*), 126.9 (d, P*Ph*), 129.5 (d, P*Ph*), 133.8 (d, P*Ph*), 134.0 (d, P*Ph*), 136.5 (q, B*Ph*), 164.6 (q, $^1J_{CB}$ = 49.4 Hz, B-*C*). ^{11}B NMR (CD$_2$Cl$_2$, 161 MHz, 298 K): δ (ppm) -5.9 (s). ^{31}P{^{1}H} NMR (CD$_2$Cl$_2$, 203 MHz, 298 K): δ (ppm) 30.2 (s). Anal. Calcd: [fc(NPPh$_3$)$_2$PdMe][BPh$_4$]·(THF)$_1$ (C$_{75}$H$_{69}$BFeN$_2$OP$_2$Pd) C, 72.10; H, 5.57; N, 2.24. Found: C, 72.13; H, 5.61; N, 2.29.

[fc(NPPh$_3$)$_2$Pd(THF)][BF$_4$]$_2$. To a suspension of AgBF$_4$ (54.4 mg, 0.279 mmol) in 2 mL of methylene chloride was added [fc(NPPh$_3$)$_2$PdMe][BPh$_4$] (116.3 mg, 0.093 mmol) in 5 mL of methylene chloride at ambient temperature. The reaction solution was stirred for 10 min at ambient temperature before being filtered through a Celite plug. The filtrate was concentrated to 2 mL followed by the addition of a few drop of THF, layering with 2 mL of diethyl ether, and stored overnight at -35 °C. Decanting of the solution and washing with cold diethyl ether yielded the product as dark golden plates (79.9 mg, 73.2%). X-ray quality crystals were obtained from a methylene chloride/THF (1:2 vol %) layering at ambient temperature. Crystals of [fc(NPPh$_3$)$_2$Pd(THF)][BF$_4$]$_2$ always contain 1.5 molecules of methylene chloride per molecule of compound as supported by NMR spectroscopic data. ^{1}H NMR (CD$_2$Cl$_2$, 500 MHz, 298 K): δ (ppm) 1.61 (m, 4H, C*H*$_2$), 3.53 (m, 4H, OC*H*$_2$), 3.63 (t, 4H, Cp-*H*), 5.39 (t, 4H, Cp-*H*), 7.66 (m, 12H, *o*-Ph), 7.75 (m, 18H, *m*-Ph, *p*-Ph). ^{13}C NMR (CD$_2$Cl$_2$, 126 MHz, 298 K): δ (ppm) 25.9 (s, *C*H$_2$), 69.1 (s, O*C*H$_2$), 73.2 (d, Cp-*C*), 83.8 (s, Cp-*C*), 106.9 (d, Cp-*C*), 123.9 (d, P*Ph*), 130.8 (d, P*Ph*), 133.3 (d, P*Ph*), 135.4 (d, P*Ph*). ^{11}B NMR (CD$_2$Cl$_2$, 161 MHz, 298 K): δ (ppm) -0.4 (br s). ^{19}F NMR spectrum (CD$_2$Cl$_2$, 282 MHz, 298 K) of [fc(NPPh$_3$)$_2$Pd(THF)][BF$_4$]$_2$: δ (ppm) -152.0 (br s), -152.1 (br s). ^{31}P{^{1}H} NMR (CD$_2$Cl$_2$, 203 MHz, 298 K): δ (ppm) 37.4 (s). Anal. Calcd: [fc(NPPh$_3$)$_2$Pd(THF)][(BF$_4$)$_2$]·(CH$_2$Cl$_2$)$_{1.5}$ (C$_{51.5}$H$_{49}$B$_2$Cl$_3$F$_8$FeN$_2$OP$_2$Pd) C, 50.86; H, 4.06; N, 2.30. Found: C, 51.20; H, 3.97; N, 2.28.

fc(NPEt$_3$)$_2$. To fc(N$_3$)$_2$ (194.0 mg, 0.724 mmol) in 8 mL of hexanes was added PEt$_3$ (0.21 mL, 1.45 mmol) in 8 mL of hexanes drop-wise under subdued light. The reaction solution was stirred for 1 h at ambient temperature. The hexanes solution was decanted and volatile substances were removed under a reduced pressure. The remaining orange crystalline solids were dissolved in 2 mL of diethyl ether, layered with 2 mL of hexanes, and stored for 18 h at -35 °C. Decanting of the solution and washing with 2 mL of cold hexanes yielded the product as red crystals (295.1 mg, 90.9%). ^{1}H NMR (CDCl$_3$, 500 MHz, 298 K): δ (ppm) 1.13 (m, 18H, CH$_2$C*H*$_3$), 1.85 (m, 12H, C*H*$_2$CH$_3$), 3.66 (t, 4H, Cp-*H*), 3.74 (t, 4H, Cp-*H*). ^{13}C NMR (CDCl$_3$, 126 MHz, 298 K): δ (ppm) 6.6 (d, CH$_2$*C*H$_3$), 18.0 (d, *C*H$_2$CH$_3$), 61.3 (d, Cp-*C*), 64.8 (s, Cp-*C*), 111.6 (s, Cp-*C*). ^{31}P{^{1}H} (CDCl$_3$, 203 MHz, 298 K): δ (ppm) 28.9 (s). Anal. Calcd: fc(NPEt$_3$)$_2$ (C$_{22}$H$_{38}$FeN$_2$P$_2$) C, 58.94; H, 8.54; N, 6.25. Found: C, 59.15; H, 8.55; N, 6.18.

fc(NPEt$_3$)$_2$PdCl(Me). To (COD)PdCl(Me) (80.2 mg, 0.303 mmol) in 3 mL of methylene chloride was added fc(NPEt$_3$)$_2$ (123.3 mg, 0.275 mmol) in 4 mL of methylene chloride and the reaction mixture was stirred for 1 h at ambient temperature. The reaction mixture was filered through Celite, volatile substances were removed under a reduced pressure, the product extracted with 5 mL of toluene. Removal of toluene under a reduced pressure yielded the product as an orange oil (120.9 mg, 72.6%). ^{1}H NMR (C$_6$D$_6$, 500 MHz, 298 K): δ (ppm) 0.72 (m, 9H, CH$_2$C*H*$_3$), 0.81 (m, 9H, CH$_2$C*H*$_3$), 1.21 (s, 3H, Pd-C*H*$_3$), 1.45 (m, 3H, C*H*$_2$CH$_3$), 1.70 (m, 6H, C*H*$_2$CH$_3$), 2.39 (m, 3H, C*H*$_2$CH$_3$), 3.75 (br s, 1H, Cp-*H*), 3.77 (br s, 1H, Cp-*H*), 3.80 (br s, 1H, Cp-*H*), 3.88 (br s, 1H, Cp-*H*), 4.05 (br s, 1H, Cp-*H*), 4.08 (br s, 1H, Cp-*H*), 5.19 (br s, 1H, Cp-*H*), 5.52 (br s, 1H, Cp-*H*). ^{13}C NMR (C$_6$D$_6$, 126 MHz, 298 K): δ (ppm) -9.8 (t, Pd-*C*H$_3$), 6.8 (d, CH$_2$*C*H$_3$), 7.2 (d, CH$_2$*C*H$_3$), 18.3 (d, *C*H$_2$CH$_3$), 18.8 (d, *C*H$_2$CH$_3$), 63.1 (s, Cp-*C*), 63.7 (s, Cp-*C*), 65.4 (s, Cp-*C*), 65.8 (s, Cp-*C*), 67.0 (s, Cp-*C*), 67.1 (s, Cp-*C*), 68.1 (s, Cp-*C*), 70.1 (s, Cp-*C*), 109.1 (d, Cp-*C*), 109.3 (m, Cp-*C*). ^{31}P{^{1}H} NMR (C$_6$D$_6$, 203 MHz, 298 K): δ (ppm) 43.3 (s), 45.1 (s). Anal. Calcd: fc(NPEt$_3$)$_2$PdCl(Me) (C$_{22}$H$_{40}$FeN$_2$P$_2$Pd) C, 45.64; H, 6.83; N, 4.63. Found: C, 45.74; H, 6.71; N, 4.72.

[fc(NPEt$_3$)$_2$PdMe][BPh$_4$]. To fc(NPEt$_3$)$_2$PdCl(Me) (156.5 mg, 0.258 mmol) in 8 mL of methylene chloride was added solid NaBPh$_4$ (88.5 mg, 0.258 mmol) and the resulting suspension stirred for 30 min at ambient temperature. The reaction

mixture was filtered through Celite followed by removal of volatile substances under reduced pressure. The remaining solids were dissolved in 2 mL of methylene chloride and layered with 6 mL of diethyl ether. Orange crystalline material forms after several hours at ambient temperature. Decanting of the solution and washing with diethyl ether yielded the product as an orange crystalline material (181.8 mg, 79.3%). X-ray quality crystals were obtained from methylene chloride/diethyl ether vapor diffusion. Crystals of [fc(NPEt$_3$)$_2$PdMe][BPh$_4$] always contain a molecule of methylene chloride per molecule of compound as supported by NMR spectroscopic data. ^{1}H NMR (CDCl$_3$, 500 MHz, 298 K): δ (ppm) 0.91 (s, 3H, Pd-C*H*$_3$), 1.09 (m, 18H, CH$_2$C*H*$_3$), 1.82 (m, 12H, C*H*$_2$CH$_3$), 2.97 (t, 4H, Cp-*H*), 4.63 (t, 4H, Cp-*H*), 6.89 (t, 4H, B-(*p*-Ph)), 7.04 (t, 8H, B-(*m*-Ph)), 7.41 (br s, 8H, B-(*o*-Ph)). ^{13}C NMR (CDCl$_3$, 126 MHz, 298 K): δ (ppm) -11.1 (t, Pd-*C*H$_3$), 6.1 (d, CH$_2$*C*H$_3$), 18.1 (d, *C*H$_2$CH$_3$), 67.5 (d, Cp-*C*), 72.5 (s, Cp-*C*), 87.6 (d, Cp-*C*), 121.8 (s, B*Ph*), 125.6 (q, B*Ph*), 136.5 (q, B*Ph*), 164.4 (q, $^1J_{CB}$ = 49.3 Hz, B-*C*). ^{11}B NMR (CDCl$_3$, 161 MHz, 298 K): δ (ppm) -5.7 (s). ^{31}P{^{1}H} NMR (CDCl$_3$, 203 MHz, 298 K): δ (ppm) 57.3 (s). Anal. Calcd: [fc(NPEt$_3$)$_2$PdMe][BPh$_4$]·(CH$_2$Cl$_2$) (C$_{48}$H$_{63}$BCl$_2$FeN$_2$P$_2$Pd) C, 59.19; H, 6.52; N, 2.88. Found: C, 59.18; H, 6.49; N, 2.78.

NMR scale polymerizations. To a small vial, [fc(NPPh$_3$)$_2$PdMe][BPh$_4$] (5 μmol), the monomer (0.5 mmol), and 0.5 mL of CD$_2$Cl$_2$ were added. The contents of the vial were stirred and the homogeneous solution was transferred to a J. Young NMR tube equipped with a Teflon valve. The NMR tube was sealed, taken out of the box and placed in an oil bath. The polymerization activity was monitored by ^{1}H NMR spectroscopy. In the case of ethylene, the J. Young NMR tube was degassed via three cycles of freeze-pump-thaw and refilled with 1.0 atm of ethylene.

Electrochemical studies. Cyclic voltammetry studies were carried out in a 20 mL scintillation vial with electrodes fixed in position by a rubber stopper, in a 0.10 M tetrabutylammonium hexafluorophosphate or tetrapropylammonium tetrakis(3,5-bis(trifluoromethyl)phenyl)borate solution in methylene chloride. A glassy carbon working electrode (planar circular area = 0.071 cm^2), a platinum reference electrode (planar circular area = 0.031 cm^2), and a silver-wire pseudo-reference electrode were purchased from CH Instruments. Before each cyclic voltammogram was recorded, the working and auxiliary electrodes were polished with an aqueous suspension of 0.05 μm alumina on a Microcloth polishing pad. Cyclic voltammograms were acquired with a CH Instruments CHI630D potentiostat and recorded with CH Instruments software (version 13.04) with data processing on Origin 9.2. All potentials are given with respect to the ferrocene-ferrocenium couple.

X-ray crystallography. X-ray quality crystals were obtained from various concentrated solutions placed in a -35 °C freezer in the glove box unless otherwise specified. Inside the glove box, the crystals were coated with oil (STP Oil Treatment) on a microscope slide, which was brought outside the glove box. The X-ray data collections were carried out on a Bruker SMART 1000 single crystal X-ray diffractometer using MoK$_\alpha$ radiation and a SMART APEX CCD detector. The data was reduced by SAINTPLUS and an empirical absorption correction was applied using the package SADABS. The structure was solved and refined using SHELXTL (Brucker 1998, SMART, SAINT, XPREP AND SHELXTL, Brucker AXS Inc., Madison, Wiscosin, USA). Tables with atomic coordinates and equivalent isotropic displacement parameters, with all the distances and angles, and with anisotropic displacement parameters are listed in the cif.

DFT calculations. All structures were optimized using the ADF2013.01 software suite.[57-59] Full molecules were used for calculations. Optimizations were performed at the PW91[60] theory level, with full electron (no frozen cores) triple-ζ-potential (TZP) basis sets and using the relativistic scalar ZORA approximation. Mayer bond orders and atomic properties were calculated using the defaults implemented in the ADF2013.01 program suite. The optimized coordinates were used for further analysis with NBO 6.0 and Bader's Atoms In Molecules (AIM) methods, implemented in ADF.

ASSOCIATED CONTENT

Supporting Information

NMR spectra, cyclic voltammograms, X-ray, and DFT calculation data. This material is available free of charge via the Internet at http://pubs.acs.org.

AUTHOR INFORMATION

The authors declare no competing financial interests.

Corresponding Author

* Email: pld@chem.ucla.edu

ACKNOWLEDGMENT

We thank the NSF, Grant 1362999 and CHE-1048804 for NMR spectroscopy.

REFERENCES

1. Blanco, V.; Leigh, D. A.; Marcos, V. *Chem. Soc. Rev.* **2015,** *44* (15), 5341-5370.
2. Teator, A. J.; Lastovickova, D. N.; Bielawski, C. W. *Chem. Rev.* **2016,** *116* (4), 1969-1992.
3. Gregson, C. K. A.; Gibson, V. C.; Long, N. J.; Marshall, E. L.; Oxford, P. J.; White, A. J. P. *J. Am. Chem. Soc.* **2006,** *128* (23), 7410-7411.
4. Broderick, E. M.; Guo, N.; Vogel, C. S.; Xu, C.; Sutter, J.; Miller, J. T.; Meyer, K.; Mehrkhodavandi, P.; Diaconescu, P. L. *J. Am. Chem. Soc.* **2011,** *133* (24), 9278–9281.
5. Süßner, M.; Plenio, H. *Angew. Chem. Int. Ed.* **2005,** *44* (42), 6885-6888.
6. Liu, G.; He, H.; Wang, J. *Adv. Synth. Catal.* **2009,** *351* (10), 1610-1620.
7. Ringenberg, M. R.; Kokatam, S. L.; Heiden, Z. M.; Rauchfuss, T. B. *J. Am. Chem. Soc.* **2007,** *130* (3), 788-789.
8. Slone, C. S.; Mirkin, C. A.; Yap, G. P. A.; Guzei, I. A.; Rheingold, A. L. *J. Am. Chem. Soc.* **1997,** *119* (44), 10743-10753.
9. Allgeier, A. M.; Mirkin, C. A. *Angew. Chem. Int. Ed.* **1998,** *37* (7), 894-908.
10. Tennyson, A. G.; Lynch, V. M.; Bielawski, C. W. *J. Am. Chem. Soc.* **2010,** *132* (27), 9420-9429.
11. Ringenberg, M. R.; Nilges, M. J.; Rauchfuss, T. B.; Wilson, S. R. *Organometallics* **2010,** *29* (8), 1956-1965.
12. Lorkovic, I. M.; Duff, R. R.; Wrighton, M. S. *J. Am. Chem. Soc.* **1995,** *117* (12), 3617-3618.
13. Leibfarth, F. A.; Mattson, K. M.; Fors, B. P.; Collins, H. A.; Hawker, C. J. *Angew. Chem. Int. Ed.* **2013,** *52* (1), 199-210.
14. Sud, D.; Norsten, T. B.; Branda, N. R. *Angew. Chem. Int. Ed.* **2005,** *44* (13), 2019-2021.
15. Wang, J.; Feringa, B. L. *Science* **2011,** *331* (6023), 1429-1432.
16. Romanazzi, G.; Degennaro, L.; Mastrorilli, P.; Luisi, R. *ACS Catal.* **2017,** *7* (6), 4100-4114.
17. Quan, S. M.; Wang, X.; Zhang, R.; Diaconescu, P. L. *Macromolecules* **2016,** *49* (18), 6768-6778.
18. Wang, X.; Thevenon, A.; Brosmer, J. L.; Yu, I.; Khan, S. I.; Mehrkhodavandi, P.; Diaconescu, P. L. *J. Am. Chem. Soc.* **2014,** *136* (32), 11264-11267.
19. Biernesser, A. B.; Delle Chiaie, K. R.; Curley, J. B.; Byers, J. A. *Angew. Chem. Int. Ed.* **2016,** *55* (17), 5251–5254.

20. Zhu, Y.; Romain, C.; Williams, C. K. *J. Am. Chem. Soc.* **2015,** *137* (38), 12179-12182.
21. Paul, S.; Romain, C.; Shaw, J.; Williams, C. K. *Macromolecules* **2015,** *48* (17), 6047-6056.
22. Romain, C.; Williams, C. K. *Angew. Chem. Int. Ed.* **2014,** *53* (6), 1607-1610.
23. Liu, B.; Cui, D.; Tang, T. *Angew. Chem. Int. Ed.* **2016,** *55* (39), 11975-11978.
24. Broderick, E. M.; Guo, N.; Wu, T.; Vogel, C. S.; Xu, C.; Sutter, J.; Miller, J. T.; Meyer, K.; Cantat, T.; Diaconescu, P. L. *Chem. Commun.* **2011,** *47*, 9897-9899.
25. Abubekerov, M.; Shepard, S. M.; Diaconescu, P. L. *Eur. J. Inorg. Chem.* **2016,** *2016* (15-16), 2634-2640.
26. Chen, M.; Yang, B.; Chen, C. *Angew. Chem. Int. Ed.* **2015,** *54* (51), 15520-15524.
27. Zou, W.; Pang, W.; Chen, C. *Inorg. Chem. Front.* **2017**, *4* (5), 795-800.
28. Feyrer, A.; Breher, F. *Inorg. Chem. Front.* **2017**, *4* (7), 1125-1134.
29. Shepard, S. M.; Diaconescu, P. L. *Organometallics* **2016,** *35* (15), 2446–2453.
30. Klenk, S.; Rupf, S.; Suntrup, L.; van der Meer, M.; Sarkar, B. *Organometallics* **2017,** *36* (10), 2026-2035.
31. Cabrera, K. D.; Rowland, A. T.; Szarko, J. M.; Diaconescu, P. L.; Bezpalko, M. W.; Kassel, W. S.; Nataro, C. *Dalton Trans.* **2017,** *47*, 5702-5710.
32. Blass, B. L.; Hernández Sánchez, R.; Decker, V. A.; Robinson, M. J.; Piro, N. A.; Kassel, W. S.; Diaconescu, P. L.; Nataro, C. *Organometallics* **2016,** *35* (4), 462-470.
33. Ringenberg, M. R.; Wittkamp, F.; Apfel, U.-P.; Kaim, W. *Inorg. Chem.* **2017,** *56* (13), 7501-7511.
34. Warnick, E. P.; Dupuis, R. J.; Piro, N. A.; Scott Kassel, W.; Nataro, C. *Polyhedron* **2016,** *114*, 156-164.
35. Gramigna, K. M.; Oria, J. V.; Mandell, C. L.; Tiedemann, M. A.; Dougherty, W. G.; Piro, N. A.; Kassel, W. S.; Chan, B. C.; Diaconescu, P. L.; Nataro, C. *Organometallics* **2013,** *32* (20), 5966–5979.
36. Gusev, O. V.; Kalsin, A. M.; Peterleitner, M. G.; Petrovskii, P. V.; Lyssenko, K. A.; Akhmedov, N. G.; Bianchini, C.; Meli, A.; Oberhauser, W. *Organometallics* **2002,** *21* (17), 3637-3649.
37. Zuideveld, M. A.; Swennenhuis, B. H. G.; Kamer, P. C. J.; van Leeuwen, P. W. N. M. *J. Organomet. Chem.* **2001,** *637-639*, 805-808.
38. Seyferth, D.; Hames, B. W.; Rucker, T. G.; Cowie, M.; Dickson, R. S. *Organometallics* **1983,** *2*, 472-474.
39. Cowie, M.; Dickson, R. S. *J. Organomet. Chem.* **1987,** *326* (2), 269-280.
40. Sato, M.; Suzuki, K.; Asano, H.; Sekino, M.; Kawata, Y.; Habata, Y.; Akabori, S. *J. Organomet. Chem.* **1994,** *470* (1), 263-269.
41. Takemoto, S.; Kuwata, S.; Nishibayashi, Y.; Hidai, M. *Inorg. Chem.* **1998,** *37* (25), 6428-6434.
42. Pick, F. S.; Thompson, J. R.; Savard, D. S.; Leznoff, D. B.; Fryzuk, M. D. *Inorg. Chem.* **2016,** *55* (8), 4059-4067.
43. Metallinos, C.; Tremblay, D.; Barrett, F. B.; Taylor, N. J. *J. Organomet. Chem* **2006,** *691* (9), 2044-2047.
44. Jess, K.; Baabe, D.; Bannenberg, T.; Brandhorst, K.; Freytag, M.; Jones, P. G.; Tamm, M. *Inorg. Chem.* **2015,** *54* (24), 12032-12045.
45. Green, A. G.; Kiesz, M. D.; Oria, J. V.; Elliott, A. G.; Buechler, A. K.; Hohenberger, J.; Meyer, K.; Zink, J. I.; Diaconescu, P. L. *Inorg. Chem.* **2013,** *52* (9), 5603–5610.
46. Duhović, S.; Oria, J. V.; Odoh, S. O.; Schreckenbach, G.; Batista, E. R.; Diaconescu, P. L. *Organometallics* **2013,** *32* (20), 6012–6021.
47. Carver, C. T.; Monreal, M. J.; Diaconescu, P. L. *Organometallics* **2008,** *27*, 363-370.
48. Shafir, A.; Arnold, J. *J. Am. Chem. Soc.* **2001,** *123* (37), 9212-9213.
49. Huang, W.; Khan, S. I.; Diaconescu, P. L. *J. Am. Chem. Soc.* **2011,** *133* (24), 10410-10413.
50. Diaconescu, P. L. *Comments Inorg. Chem.* **2010,** *31* (5-6), 196-241.
51. Diaconescu, P. L. *Acc. Chem. Res.* **2010,** *43* (10), 1352-1363.
52. Monreal, M. J.; Diaconescu, P. L. *Organometallics* **2008,** *27*, 1702-1706.
53. Monreal, M. J.; Carver, C. T.; Diaconescu, P. L. *Inorg. Chem.* **2007,** *46*, 7226-7228.
54. Otón, F.; Ratera, I.; Espinosa, A.; Wurtz, K.; Parella, T.; Tárraga, A.; Veciana, J.; Molina, P. *Chem. Eur. J.* **2010,** *16* (5), 1532-1542.
55. Yang, L.; Powell, D. R.; Houser, R. P. *Dalton Trans.* **2007,** (9), 955-964.
56. Sato, M.; Shigeta, H.; Sekino, M.; Akabori, S. *J. Organomet. Chem.* **1993,** *458* (1-2), 199-204.
57. ADF2013.01; SCM Scientific Computing & Modeling: Theoretical Chemistry, Vrije Universiteit, Amsterdam, The Netherlands.
58. te Velde, G.; Bickelhaupt, F. M.; Baerends, E. J.; Fonseca Guerra, C.; van Gisbergen, S. J. A.; Snijders, J. G.; Ziegler, T. *J. Comput. Chem.* **2001,** *22* (9), 931-967.
59. Fonseca Guerra, C.; Snijders, J. G.; te Velde, G.; Baerends, E. J. *Theor. Chem. Acc.* **1998,** *99*, 391-403.
60. Perdew, J. P.; Wang, Y. *Phys. Rev. B* **1992,** *45* (23), 13244-13249.
61. Mayer, I. *Int. J. Quantum Chem.* **1984,** *26* (1), 151-154.
62. Bridgeman, A. J.; Cavigliasso, G.; Ireland, L. R.; Rothery, J. *J. Chem. Soc., Dalton Trans.* **2001,** (14), 2095-2108.
63. Glendening, E. D.; Badenhoop, J. K.; Reed, A. E.; Carpenter, J. E.; Bohmann, J. A.; Morales, C. M.; Landis, C. R.; Weinhold, F. *http://nbo6.chem.wisc.edu: Theoretical Chemistry Institute, University of Wisconsin, Madison, WI*, 2013.
64. Bader, R. F. W., *Atoms in Molecules - A Quantum Theory*. Oxford University Press: Oxford, 1990.
65. Rodríguez, J. I.; Bader, R. F. W.; Ayers, P. W.; Michel, C.; Götz, A. W.; Bo, C. *Chem. Phys. Lett.* **2009,** *472* (1-3), 149-152.
66. Fowe, E. P.; Therrien, B.; Suss-Fink, G.; Daul, C. *Inorg. Chem.* **2007,** *47* (1), 42-48.
67. Makal, A. M.; Plażuk, D.; Zakrzewski, J.; Misterkiewicz, B.; Woźniak, K. *Inorg. Chem.* **2010,** *49* (9), 4046-4059.
68. Pangborn, A. B.; Giardello, M. A.; Grubbs, R. H.; Rosen, R. K.; Timmers, F. J. *Organometallics* **1996,** *15* (5), 1518-1520.
69. Zeller, A.; Herdtweck, E.; Strassner, T. *Eur. J. Inorg. Chem.* **2003,** *2003* (9), 1802-1806.
70. Shafir, A.; Power, M. P.; Whitener, G. D.; Arnold, J. *Organometallics* **2000,** *19* (19), 3978-3982.
71. Dhar, D.; Yee, G. M.; Spaeth, A. D.; Boyce, D. W.; Zhang, H.; Dereli, B.; Cramer, C. J.; Tolman, W. B. *J. Am. Chem. Soc.* **2016,** *138* (1), 356-368.

TOC graphic

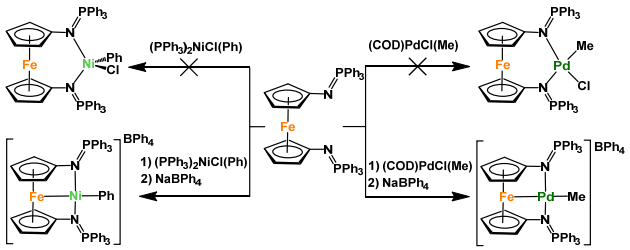
(PPh3)2NiCl(Ph)
(COD)PdCl(Me)
1) (PPh3)2NiCl(Ph)
2) NaBPh4
1) (COD)PdCl(Me)
2) NaBPh4